Forward Modeling of Frequency-domain Helicopter-borne Electromagnetic Data using an Improved Finite Difference Method

Saeed Nazari, Alireza ArabAmiri*, Abolghasem Kamkar Rouhani, and Fereydoun Sharifi

School of Mining, Petroleum and Geophysics Engineering, Shahrood University of Technology, Shahrood, Iran

Article Info	Abstract

Abstract

In this work, we simulate the frequency-domain helicopter-borne electromagnetic (HEM) data over the two-dimensional (2D) and three-dimensional (3D) earth models. In order to achieve this aim, the vector Helmholtz equation is used to avoid the convergence problems in Maxwell's equations, and the corresponding fields are divided into primary and secondary components. We use the finite difference method on a staggered grid to discretize the equations, which can be performed in two ways including the conventional and improved finite difference methods. The former is very complex in terms of programming, which causes errors. Furthermore, it requires different programming loops over each point of the grid, which increases the program's running time. The latter is the improved finite difference method (IFDM), in which pre-made derivative matrices can be used. These pre-made derivative matrices can be incorporated into the derivative equations and convert them directly from the derivative form to the matrix form. After having the matrix form system of linear equations, Ax = b is solved by the quasi-minimal residual (QMR). IFDM does not have the complexities of the conventional method, and requires much less execution time to form a stiffness or coefficient matrix. Moreover, its programing process is simple. Our code uses parallel computing, which gives us the ability to calculate the fields for all transmitter positions at the same time, and because we use sparse matrices thorough the code memory space, requires to store the files is less than 100 MB compared with normal matrices that require more than 15 GB space in the same grid size. We implement IFDM to simulate the earth's responses. In order to validate, we compare our results with various models including the 3D and 2D models, and anisotropic conductivity. The results show a good fit in comparison with the FDM solution of Newman and the appropriate fit integral equations solution of Avdeev that is because of the different solution methods.

1. Introduction

The frequency-domain helicopter-borne electromagnetic (HEM) method is extensively used in a wide range of geoscience fields. Peltoniemi studied the depth of investigation of a fixed-wing frequency-domain airborne electromagnetic system, and based on his work and the modeling output, the depth of penetration in resistive topography for the airborne system was between 85 m and 210 m depending on the geometry and the size of the conductive body. Host rock and overburden of low but finite conductivity do not make a significant change in the penetration depth. The screening and the attenuation effects from conductive overburden and conductive host rock will, however, decrease the depth of penetration [1]. Kokpiang used airborne electromagnetic data to map groundwater salinity and salt store at Chowilla. They performed a HEM survey, and proved the ability of airborne electromagnetic combined with pore fluid salinity data and predicted the groundwater salinity and salt store distribution across the floodplain. [2]. Siemon created the work frame of frequency-domain helicopter-borne electromagnetics for groundwater exploration in urban areas. By using high-frequency data, they described the shallower parts

✉ *Corresponding author: alirezaarabamiri@yahoo.com (A.R. ArabAmiri)*

of the conducting subsurface or highly conductive saltwater-saturated sediments and the low-frequency data the deeper parts of resistive hard rocks in urban areas, despite a few man-made sources that affect the field measurements [3], and Baranwal used 3D interpretation of frequency domain (HEM) data to study the Mesozoic sedimentary basin to delineate the extent of the sedimentary basin and found highly conductive areas using HEM data interpretation. In one of these areas, graphite and sulfide mineral outcrops were found by field observations [4].

To interpret the HEM data, substantial efforts have been made to perform the one-dimensional (1-D) [5; 6; 7; 8; 9, 10; 11;12], 2D [13; 14; 15; 16; 17; 18; 19; 20; 21; 22; 23; 24)] as well as 3D [25; 26; 27; 28; 29; 30] numerical modeling of the respective data. Various numerical methods have been implemented by pioneer researchers such as Coggon (1971) that computed electromagnetic responses of two-dimensional structures, with line source excitation including the effects of adjacent conductors and magnetic conductors set in a less conductive half-space by the finite element method to simulate complex structures [31]. Xiong (1992) simulated responses of 3-D structures by the method of system iteration using integral equations [32]. Newman (1995) used staggered finite differences for modelling of airborne electromagnetic responses in frequency-domain [33]. Habashy (1993) by using a non-linear method calculated the electromagnetic scattering [34] [e.g. 35; 36; 37].

Since in most cases the earth has a two/three-dimensional (2-D/3-D) structure and is inherently associated with complexities, 1-D modeling cannot provide a reliable result [38; 39], and therefore, a 2-D/3-D modeling has to be executed to model the HEM data acquired above that [38].

Numerous attempts have been made to perform the forward-modeling using the finite difference method (FDM) [24; 33; 40; 41], finite element method (FEM) [19; 20; 27; 42; 43; 44; 45], finite volume method (FVM) [46; 47; 48; 49; 50], integral equations (IQ) [39; 51; 52], and hybrid of numerical method [53; 54].

Moreover, high computational volume and the need for huge processing memory is one of the most important problems of the finite element method [25; 55]. The finite difference methods are effective from the point of view of the simplicity of the discretization algorithm to create the coefficient matrix and the models that are not too complex [56].

To solve the Maxwell equations using the FDM method, the differential equations have to be discretized numerically. In order to discretize the Maxwell equation, two general methods including the staggered grid and non-staggered grid were presented by Yee [57]. One of the most important deficiencies of the non-staggered method is the large calculation and dealing with large dimensional matrices. However, the staggered scheme does not suffer from this problem [58]. Furthermore, using the staggered grid divergence equations is naturally satisfied and the boundary conditions, which can be attributed to each of the grid cells of the desired conductivity, are well-satisfied.

However, the conventional approach of 2-D and 3-D programming of the staggered grid is really challenging and prone to errors and bugs. In addition, this discrete form of the equation needs to be calculated for every point in the grid, which is relatively expensive computationally. To deal with these problems, we use an improved finite difference method (IFDM), which has been developed by Rumpf [59; 60] and has not been used for modeling the geophysical electromagnetic data so far. In this method, some derivative matrices are built, and then these pre-made matrices are incorporated into the derivative equations and convert them directly from the derivative form to the matrix form. The result of this procedure is a system of linear equations. This method is easy to program and very fast, and does not have the complexity of the conventional method [59, 60].

We found that the execution times of this method to build the left-hand side (LHS) matrix and curl calculation of a 3-D model with the dimension of 700m*500m*500m and a mesh size of 5m*5m*5m using a computer with a configuration of a processor of 16 cores (2.5 GHz) and 64 GB RAM, are 14 and 3 seconds, respectively. However, in the case of using the conventional method, the elapsed time for these calculations is almost 7 hours. In terms of Ram usage, improved method used 48 GB of Ram for 14 and 3 seconds but the conventional method used 48 GB of Ram for almost 7 hours; on the other hand, because we use sparse matrices throughout the code, it only requires less than 100 MB of memory space, compared to the conventional matrices that require more than 15 GB.

2. Methodology
2.1. Electromagnetic equations

The propagation of EM waves is based on the Maxwell's equations [61].

The desired HEM responses for the simulation must be calculated with the magnetic dipole source affecting the receiver. This greatly complicates solutions because the fields close to the source are changing rapidly. Therefore, in the case of using a very large mesh, the numerical difference at the receiver is prone to inaccuracy. However, using a very fine grid near the source and receiver cause problem and limits the size of the model because there is a limitation in computer storage. In order to overcome this problem, the fields are divided into primary and secondary fields (1) [33; 62]. Thereby, the numerical solutions are divided into two parts, and primary fields can be calculated analytically. Thus singular point source is removed from the numerical solution [33; 19; 20].

$$e = e_{primary} + e_{secondary}$$
$$\sigma = \sigma_{primary} + \sigma_{secondary} \tag{1}$$

where e and σ stand for electrical field and conductivity, respectively.

From the Maxwell equations, the secondary electric field can be derived as follows [23; 29]:

$$\nabla_h \times \nabla_e \times e_{sec} + i\,\omega\mu_0\sigma e_{sec} = -i\,\omega\mu_0\sigma_{sec}e_{pri} \tag{2}$$

where e_{pri} is the primary electric field arising from a dipole source or analytic whole space source. $\omega = 2\pi f$ is the angular frequency, and μ is the magnetic permeability. Now that we have our equation, the next step is to approximate the electric field using finite difference on a staggered grid scheme. There are two approaches that we can use in this regard: the conventional finite difference method and the improved finite difference method.

2.2. Finite difference method (FDM)

In general, we start with the governing equation. Equations 3-21 are simple general math examples to make the concept easier to understand or system of governing equations, for example, Equation (3), and we have some other information like boundary values and certain range that we are interested in, and somehow define the problem. This is where we apply FDM and approximate the derivatives, make

function y discrete after that we get a system of equations write that finite difference equation once for every point in the grid, and put that set of equations in matrix form (4). Thus FDM is what takes us from our analytical differential equation to the matrix form, and after that we can just think of this y as our unknown, and if we solve that for y, we will get our answer (5).

$$\frac{d^2}{dx^2}y(x) - \frac{d}{dx}y(x) + y(x) = 0$$
$$0 \le x \le 10 \tag{3}$$
$$y(0) = 1, y(10) = 5$$

$$[A][y] = [b] \tag{4}$$

$$[y] = [A]^{-1}[b] \tag{5}$$

In the conventional FDM, we have our governing Equation (3); the first step is making this equation discrete (6); here is an important part of writing finite difference equations. Every single term must exist at the same point in space so now our function y will only exist at discrete values x, which allows us then to use FDM. However, in the computer code, we are working with a range where we have our first, second, third, and fourth element and so on, and it is better to write difference equations in array indices (7), and now "i" is an integer that goes from one all the way to the number of points on the grid. The next step is rearranging the finite difference equation, so in its present form (7), our finite differences are quite apparent; however, we have to build a giant matrix, and it will be a lot easier to do that if we rearrange this to become (8). The next step is to set up the grid and calculate the grid parameters like grid spacing Δx and after that, we can put this value in (8) and end up with a simple equation; for example, if we have a 21-point grid, which means we have 20 spaces equation becomes (9) but this equation is very specific to that grid that has a spacing of 0.5 and if spacing changes, clearly, the numbers in that equation have to change. This equation is going to enforce our original differential equation, and we will have written that equation for every single point of our 21 points across space except the boundary values that were given to us at the beginning.

$$\frac{y(x+\Delta x)-2y(x)+y(x-\Delta x)}{\Delta x^2}-\frac{y(x+\Delta x)-y(x-\Delta x)}{2\Delta x}+y(x)=0 \tag{6}$$

$$\frac{y_{i+1}-2y_i+y_{i-1}}{\Delta x^2}-\frac{y_{i+1}-y_{i-1}}{2\Delta x}+y_i=0 \tag{7}$$

$$\left(\frac{1}{\Delta x^2}+\frac{1}{2\Delta x}\right)y_{i-1}+\left(1-\frac{2}{\Delta x^2}\right)y_i+\left(\frac{1}{\Delta x^2}-\frac{1}{2\Delta x}\right)y_{i+1}=0 \tag{8}$$

$$5y_{i-1}-7_i+3y_{i+1}=0 \Rightarrow \Delta x=0.5 \tag{9}$$

Let's repeat everything we just did with the improved finite difference method. We have the same starting point, the same governing equations, and the same boundary values; we solve the same problem just with a different way of implementing the finite difference method. What we will do for formulation rather than go through whole the complexities of the conventional method, we will just be going to go term by term and immediately write our differential equation (3) in matrix form (10). We already know that our unknown function $y(x)$ is always going to be stored as a column vector likewise zeros (excitation or source in HEM). These are the only two things ever in the differential equation that are stored as a column vector. Everything else is not a function; everything else is something operating onto those functions, and they are stored in square matrices. In the first term of Equation (3), we have a second-order derivative operating on y, so we are going to have some kind of square matrix (D_x) operating on y and what we will do is factor out the y (11) and call the matrix A, the left-hand side (LHS) matrix, and so what we have in our MATLAB code is just a line of code, and the only thing that needs to discuss, is how to build these derivative matrices and what we do is program a function in MATLAB where we tell the size of the grid and the spacing that's all the information it needs, and it will build the matrices for us and building these matrices is also very simple. We can just type in the differential equation (A=DX2−DX+I), and we are no longer even explicitly toughing finite differences and all the tediousness of the finite difference's method has gotten absorbed into that functions that build derivative matrices. Thus if you have any new differential equations, just write the LHS or A and run the code again whereas if you applying the conventional FDM, you should start approximate with finite differences, make sure all the terms exist at the same point in space, maybe you have to modify those, write it in array form then rearrange to collect terms for constant y terms, put the value for Δx to get an equation with coefficients, build your matrix then go back incorporate boundary values, then finally solve it. Its hugely complicated and even more complicated for 2D or 3D sets of differential equations, this conventional approach is very difficult and prone to errors and bugs in writing the code.

$$\left[D_x^2\right][y]-[D_x][y]+[y]=[0] \tag{10}$$

$$\left(\left[D_x^2\right]-[D_x]+[I]\right)[y]=[0]\Rightarrow[A][y]=[0] \tag{11}$$

2.3. Multivariable finite difference method

Assuming electric field e and magnetic field h and very basic multi-variable problem (12), and two unknown functions $e(x)$ and $h(x)$, if just approximate this with finite differences, it becomes in form (13); it will work but the problem is we spanning this grid by distance of $2\Delta x$ and go farther out on the grid to calculate finite differences so it will be less accurate. There is something better we can do in this case where we only have to reach Δx and if those function values are tighter against where we are calculating that finite-difference that will improve our accuracy. Thus let's only use e and h where they are defined and tighten up those finite differences so they only span one Δx and end up Equation (14); in this case we are breaking an important rule that all terms in a finite difference equation must exist at the same point in space. Thus these finite differences are defined at $(x+\Delta x)/2$, whereas $h(x)$ is happening at x and it can make the code unstable.

$$\frac{\partial e(x)}{\partial x} = ah(x)$$
$$\frac{\partial h(x)}{\partial x} = be(x)$$ (12)

$$\frac{e(x+\Delta x)-e(x-\Delta x)}{2\Delta x} = ah(x)$$
$$\frac{h(x+\Delta x)-h(x-\Delta x)}{2\Delta x} = be(x)$$ (13)

$$\frac{e(x+\Delta x)-e(x)}{\Delta x} = ah(x)$$
$$\frac{h(x+\Delta x)-h(x)}{\Delta x} = be(x)$$ (14)

2.4. Staggered grid

If we define e to exist at the integer steps of Δx and h exist at $x + \Delta x /2$, the whole Equation (15) works fine and we should remember that e and h are at physically different points. Thus if we want taking derivative of e, we are looking at the finite difference between $e(x)$ and $e(x+\Delta x)$ and interpreting that as the central difference that exists at the middle; likewise, when we are calculating the derivative of h using finite difference using $h(x+\Delta x/2)$ and $h(x+3\Delta x/2)$ and interpret that as central difference, it exists at the midpoint where e exist (Figure 1).
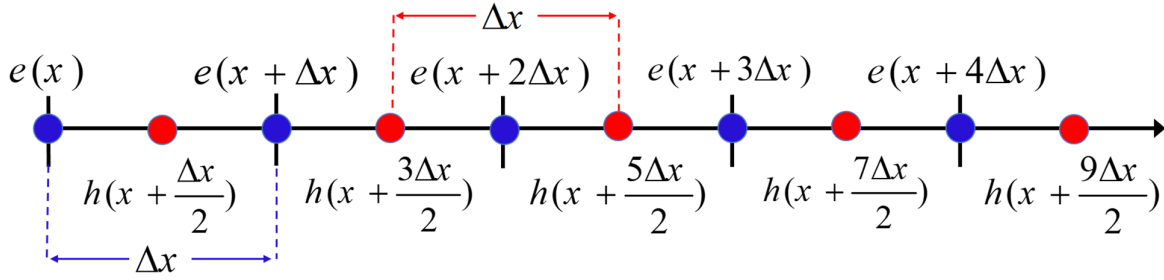

Figure 1. 1D staggered grid.

$$\frac{e(x+\Delta x)-e(x)}{\Delta x} = ah(x+\frac{\Delta x}{2})$$
$$\frac{h(x+\frac{\Delta x}{2})-h(x-\frac{\Delta x}{2})}{\Delta x} = be(x)$$ (15)

In reality, we are working with array indices in computer memory, so (15) becomes (16) and we should remember that e_i and h_i are in the same

cell in the grid and physically different positions, meaning it is staggered; they are offset by half cell (Figure 2). Due to the staggering these finite differences are written a little bit differently, in the first differential equation we have e at the next cell minus e at the same cell; this is called right derivative matrices that reaches right to calculate the finite differences but in second differential equation is h at same cell minus h at previous cell that is called left derivative matrices.
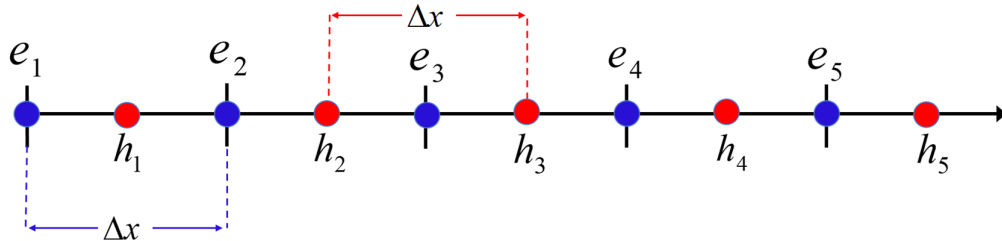

Figure 2. 1D staggered grid e_i **and** h_i **are in the same cell in the grid and physically different position.**

$$\frac{e_{i+1} - e_i}{\Delta x} = ah_i$$

$$\frac{h_i - h_{i-1}}{\Delta x} = be_i \tag{16}$$

2.5. Derivative matrices for staggered grid

Assume we have that has five cells (Figure 2) and want to write both of our finite difference equations once for each cell in the grid; this means that we will end up with ten equations (17, 18). Our first finite difference equations give us five equations and the last equation is trying to access an e_6 because we need a derivative on top of h_5, and now we have boundary condition problem; notice when we are taking the derivatives of e, there is no boundary condition problem at the first point, and this is because the staggered grid boundary condition problems only arise at one side of the grid. For our second finite difference equations that are associated with g at the first point, we are trying to calculate a derivative at e_1 that needs to reach out to the left side out of the grid that does not exist, boundary condition problems this time on different side of the grid. Here, we use the Dirichlet boundary condition, so $e_6 = 0, h_0 = 0$. We can put these sets of equations in matrix form, and stores our unknown functions in column vector e and derivative matrix D_x^e means derivative matrix operating on e in x direction and D_x^h means derivative matrix operating on h in x direction. Thus we can write Equation (12) directly in matrix form (21) and put them into a two-by-two block matrix and solve that simultaneously. $[0]$ is excitation. Important notice: these two derivative matrices are related by $\left[D_x^h\right] = -\left[D_x^e\right]^H$. It means that we only need to build one of these derivative matrices and calculate the other one immediately from it and it is just one line of code in MATLAB.

$$\frac{e_2 - e_1}{\Delta x} = ah_1$$

$$\frac{e_3 - e_2}{\Delta x} = ah_2$$

$$\frac{e_{i+1} - e_i}{\Delta x} = ah_i \Rightarrow \frac{e_4 - e_3}{\Delta x} = ah_3 \tag{17}$$

$$\frac{e_5 - e_4}{\Delta x} = ah_4$$

$$\frac{\boxed{e_6} - e_5}{\Delta x} = ah_5$$

$$\frac{h_1 - \boxed{h_0}}{\Delta x} = be_1$$

$$\frac{h_2 - h_1}{\Delta x} = be_2$$

$$\frac{h_i - h_{i-1}}{\Delta x} = be_i \Rightarrow \frac{h_3 - h_2}{\Delta x} = be_3 \tag{18}$$

$$\frac{h_4 - h_3}{\Delta x} = be_4$$

$$\frac{h_5 - h_4}{\Delta x} = be_5$$

$$\frac{1}{\Delta x}\begin{bmatrix} -1 & 1 & 0 & 0 & 0 \\ 0 & -1 & 1 & 0 & 0 \\ 0 & 0 & -1 & 1 & 0 \\ 0 & 0 & 0 & -1 & 1 \\ 0 & 0 & 0 & 0 & -1 \end{bmatrix}\begin{bmatrix} e_1 \\ e_2 \\ e_3 \\ e_4 \\ e_5 \end{bmatrix} = a\begin{bmatrix} h_1 \\ h_2 \\ h_3 \\ h_4 \\ h_5 \end{bmatrix} \tag{19}$$

$$\left[D_x^e\right][e] = a[h]$$

$$\frac{1}{\Delta x}\begin{bmatrix} 1 & 0 & 0 & 0 & 0 \\ -1 & 1 & 0 & 0 & 0 \\ 0 & -1 & 1 & 0 & 0 \\ 0 & 0 & -1 & 1 & 0 \\ 0 & 0 & 0 & -1 & 1 \end{bmatrix}\begin{bmatrix} h_1 \\ h_2 \\ h_3 \\ h_4 \\ h_5 \end{bmatrix} = b\begin{bmatrix} e_1 \\ e_2 \\ e_3 \\ e_4 \\ e_5 \end{bmatrix} \tag{20}$$

$$\left[D_x^h\right][h] = b[e]$$

$$\begin{matrix}\left[D_x^e\right][e] = a[h] \\ \left[D_x^h\right][h] = b[e]\end{matrix} \Rightarrow \begin{bmatrix} \left[D_x^e\right] & -a[I] \\ -b[I] & \left[D_x^h\right] \end{bmatrix}\begin{bmatrix} [e] \\ [h] \end{bmatrix} = \begin{bmatrix} [0] \\ [0] \end{bmatrix} \tag{21}$$

2.5.1. 2D derivative matrices for staggered grid

Assume a three by three grid (Figure 3) for building D_x^e; derivative of e function in x direction (22) [59; 60] also called right-handed

derivative matrix and we are using jacent e values so finite-difference end up at the midpoint, and that is leading to the staggering that we put h function at the midpoint of e. The red arrow point to where the derivative is being evaluated and the box encompasses the point at which we are calculating the finite difference; in the 6th equation, we are evaluating a derivative that is from outside of the grid, which means we need a function value from farther outside of the grid, and we do not have this function value and we are going to apply simple Dirichlet boundary conditions, and that means any function value from outside of the grid is zero. Notice boundary conditions problem only happened at one side of the grid (right-side), and when we calculate derivatives for h or D_x^h boundary conditions, problem still happens on one side of the grid but this time left side, so they have symmetric boundary conditions problem, whereas in the co-located grids, we have the boundary conditions problem at both sides. In the next step, we calculate the right-handed derivative matrix D_y^e, derivative of e function but this is with respect to y, so taking derivatives in vertical direction (23) [59; 60] and for example in the 8th equation, we have boundary conditions problem so we are using Dirichlet boundary conditions and as you can see boundary conditions problem only

happened at one side of the grid. The next step is to put our equation in matrix forms so that we can have a derivative matrix that will calculate the first-order derivative of functions with respect to x or y (24.25) [59; 60], and with the same process, we can build derivative matrices for 3D grids and D_z^e. As you can see, these matrices are very easy to construct in few lines of code and they have boundary conditions in them and that is zeros separate numbers by grid size. In the same way, we can build the left-handed derivative matrix for h in x and y directions or D_x^h and D_y^h also simply use one line of code and build them directly from D_x^e, D_y^e and D_z^e, they have relations of $\left[D_x^h \right] = -\left[D_x^e \right]^H$, $\left[D_y^h \right] = -\left[D_y^e \right]^H$ and $\left[D_z^h \right] = -\left[D_z^e \right]^H$ [59; 60].

As you saw, approximation using the improved FDM is very easy and straightforward, and it does not have the complex process of the conventional method; also it can run in fewer programming lines than the conventional method whereas conventional method the code must be executed for all points of grid meaning you should have for loops to build LHS and Curl operator and loop should run thousands of times.
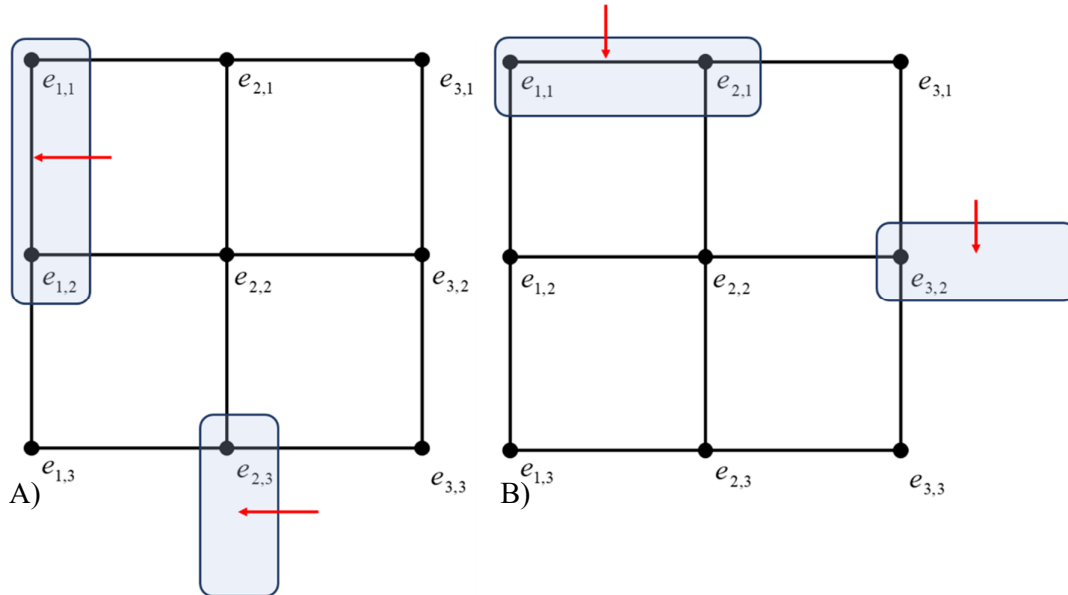

Figure 3. 2D 3by3 grid. A- Derivative in Y direction B- Derivative in X direction.

$$\frac{\partial e_{i,j}}{\partial x} \cong \frac{e_{i+1,j} - e_{i,j}}{\Delta x} \Rightarrow$$

$$\boxed{\frac{\partial e_{1,1}}{\partial x} \cong \frac{e_{2,1} - e_{1,1}}{\Delta x}}$$

$$\frac{\partial e_{2,1}}{\partial x} \cong \frac{e_{3,1} - e_{2,1}}{\Delta x}$$

$$\frac{\partial e_{3,1}}{\partial x} \cong \frac{0 - e_{3,1}}{\Delta x}$$

$$\frac{\partial e_{1,2}}{\partial x} \cong \frac{e_{2,2} - e_{1,2}}{\Delta x}$$

$$\frac{\partial e_{2,2}}{\partial x} \cong \frac{e_{3,2} - e_{2,2}}{\Delta x} \qquad (22)$$

$$\boxed{\frac{\partial e_{3,2}}{\partial x} \cong \frac{0 - e_{3,2}}{\Delta x}}$$

$$\frac{\partial e_{1,3}}{\partial x} \cong \frac{e_{2,3} - e_{1,3}}{\Delta x}$$

$$\frac{\partial e_{2,3}}{\partial x} \cong \frac{e_{3,3} - e_{2,3}}{\Delta x}$$

$$\frac{\partial e_{3,3}}{\partial x} \cong \frac{0 - e_{3,3}}{\Delta x}$$

$$\frac{\partial e_{i,j}}{\partial y} \cong \frac{e_{i,j+1} - e_{i,j}}{\Delta y} \Rightarrow$$

$$\boxed{\frac{\partial e_{1,1}}{\partial y} \cong \frac{e_{1,2} - e_{1,1}}{\Delta y}}$$

$$\frac{\partial e_{2,1}}{\partial y} \cong \frac{e_{2,2} - e_{2,1}}{\Delta y}$$

$$\frac{\partial e_{3,1}}{\partial y} \cong \frac{e_{3,2} - e_{3,1}}{\Delta y}$$

$$\frac{\partial e_{1,2}}{\partial y} \cong \frac{e_{1,3} - e_{1,2}}{\Delta y}$$

$$\frac{\partial e_{2,2}}{\partial y} \cong \frac{e_{2,3} - e_{2,2}}{\Delta y} \qquad (23)$$

$$\frac{\partial e_{3,2}}{\partial y} \cong \frac{e_{3,3} - e_{3,2}}{\Delta y}$$

$$\frac{\partial e_{1,3}}{\partial y} \cong \frac{0 - e_{1,3}}{\Delta y}$$

$$\boxed{\frac{\partial e_{2,3}}{\partial y} \cong \frac{0 - e_{2,3}}{\Delta y}}$$

$$\frac{\partial e_{3,3}}{\partial y} \cong \frac{0 - e_{3,3}}{\Delta y}$$

Dirichlet boundary conditions

Size of grid in x direction

$$\frac{1}{\Delta x}\begin{bmatrix} -1 & 1 & & & & & & & \\ & -1 & 1 & & & & & & \\ & & -1 & 0 & & & & & \\ & & & -1 & 1 & & & & \\ & & & & -1 & 1 & & & \\ & & & & & -1 & 0 & & \\ & & & & & & -1 & 1 & \\ & & & & & & & -1 & 1 \\ & & & & & & & & -1 \end{bmatrix}\begin{bmatrix} e_{1,1} \\ e_{2,1} \\ e_{3,1} \\ e_{1,2} \\ e_{2,2} \\ e_{3,2} \\ e_{1,3} \\ e_{2,3} \\ e_{3,3} \end{bmatrix} = \frac{1}{\Delta x}\begin{bmatrix} e_{2,1} - e_{1,1} \\ e_{3,1} - e_{2,1} \\ 0 - e_{3,1} \\ e_{2,2} - e_{1,2} \\ e_{3,2} - e_{2,2} \\ 0 - e_{3,2} \\ e_{2,3} - e_{1,3} \\ e_{3,3} - e_{2,3} \\ 0 - e_{3,3} \end{bmatrix} \qquad (24)$$

$$\frac{1}{\Delta y}\begin{bmatrix} -1 & 0 & 0 & 1 & & & & & \\ & -1 & 0 & 0 & 1 & & & & \\ & & -1 & 0 & 0 & 1 & & & \\ & & & -1 & 0 & 0 & 1 & & \\ & & & & -1 & 0 & 0 & 1 & \\ & & & & & -1 & 0 & 0 & 1 \\ & & & & & & -1 & 0 & 0 \\ & & & & & & & -1 & 0 \\ & & & & & & & & -1 \end{bmatrix}\begin{bmatrix} e_{1,1} \\ e_{2,1} \\ e_{3,1} \\ e_{1,2} \\ e_{2,2} \\ e_{3,2} \\ e_{1,3} \\ e_{2,3} \\ e_{3,3} \end{bmatrix} = \frac{1}{\Delta y}\begin{bmatrix} e_{1,2} - e_{1,1} \\ e_{2,2} - e_{2,1} \\ e_{3,2} - e_{3,1} \\ e_{1,3} - e_{1,2} \\ e_{2,3} - e_{2,2} \\ e_{3,3} - e_{3,2} \\ 0 - e_{1,3} \\ 0 - e_{2,3} \\ 0 - e_{3,3} \end{bmatrix} \qquad (25)$$

3. Assembling Left-hand Side of Equation

Considering the Helmholtz equation of the secondary field (2) with directly replacing derivative matrices for electric and magnetic fields, we can have block matrix LHS (29) and complete Helmholtz equation in the matrix form (30). A linear system of equations results where the matrix LHS is complex symmetric and sparse with dimensions $(3 \times N_x \times N_y \times N_z)^2$, as illustrated in Figure 4 for a 3by3by3 grid (equations 26-30 are part of our work).

$$C_e = \begin{bmatrix} 0 & -D_z^e & D_y^e \\ D_z^e & 0 & -D_x^e \\ -D_y^e & D_x^e & 0 \end{bmatrix} \tag{26}$$

$$C_h = \begin{bmatrix} 0 & -D_z^h & D_y^h \\ D_z^h & 0 & -D_x^h \\ -D_y^h & D_x^h & 0 \end{bmatrix} \tag{27}$$

$$\sigma = \begin{bmatrix} \sigma_x & 0 & 0 \\ 0 & \sigma_y & 0 \\ 0 & 0 & \sigma_z \end{bmatrix} \tag{28}$$

$$LHS = C_e C_h + i\,\omega\mu\sigma = \begin{bmatrix} -D_z^h D_z^e - D_y^h D_y^e + i\,\omega\mu\sigma_x & D_y^h D_x^e & D_z^h D_x^e \\ D_x^h D_y^e & -D_z^h D_z^e - D_x^h D_x^e + i\,\omega\mu\sigma_y & D_z^h D_y^e \\ D_x^h D_z^e & D_y^h D_z^e & -D_y^h D_y^e - D_x^h D_x^e + i\,\omega\mu\sigma_z \end{bmatrix} \tag{29}$$

$$[LHS]\begin{bmatrix} e_x^s \\ e_y^s \\ e_z^s \end{bmatrix} = -i\,\omega\mu \begin{bmatrix} \sigma_x^s & 0 & 0 \\ 0 & \sigma_y^s & 0 \\ 0 & 0 & \sigma_z^s \end{bmatrix} \begin{bmatrix} e_x^p \\ e_y^p \\ e_z^p \end{bmatrix} \tag{30}$$
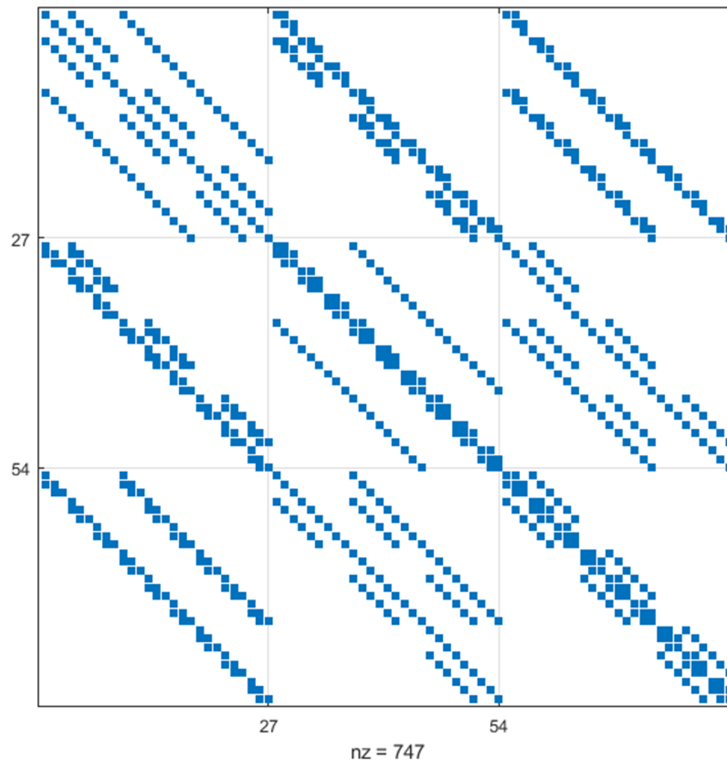

Figure 4. Structure appearance of LHS matrix for 3by3by3 staggered grid.

Many geo-physical studies involve boundary value problems arising in simulating electromagnetic fields for geological prospecting and sub-surface imaging of electrical resistivity. Simulating complex geological earth with three-dimensional finite-difference grids ends up in large sparse linear systems of equations $Ax = b$. For solving this kind of system, we used the iterative Krylov methods. Time-harmonic modeling of eddy currents is commonly carried out using the QMR method [e.g. 63; 64; 65; 66]. Unlike typical engineering applications, geo-physical electromagnetic responses are based on the Maxwell's equations in the quasi-static limit, where EM diffusion dominates [67]. We describe the earth's conductivity (or resistivity) by the diagonal tensor 28. After obtaining the secondary electric fields, by numerically approximating the curl of the electric field on the grid; the magnetic field can be calculated and then interpolated into the desired location using the spline interpolation method.

3.1. Algorithm

In terms of algorithm after inputting geometrical and physical parameters and start the program, based on the dimension of the calculation world,

LHS and Curl operator will create and save; these matrices are just created once and save will be used in the entire forward modelling unless we change the dimension of the world. It is worth mentioning that we use sparse matrices throughout the code, and using this type of matrices has a great impact on the space and time required for saving files so that it needs less than 100 MB memory to save files. In the next step, based on cells dimensions and conductivity create world function perform a averaging. The weighting factors are given by the ratio of a single cell volume to the total volume of the four adjacent cells that surround a node; these matrices will be created once and used throughout the forward problem.

In the next step, with source position primary field calculate in every point of the grid then using QMR method secondary electric field obtain and after performing Curl and interpolation secondary magnetic field for the desired receiver position is calculated. Because our code works with parallel computing and we already have the required matrices such as LHS, Curl, world we can calculate the fields for all transmitter points at the same time and this feature of our code has great impact on time. In the following you can see some parts of the code.

Inputs:

```
D_P=; %dipole type    'VMD' or 'HMD'

X=; % length of the world in X direction
Y=; % length of the world in Y direction
Z=; % length of the world in Z direction


%%%%%%%%%%%%%%%%%%%%%%%%%%%%%%%%%%%%%%%%% MESH SETTING

dx_a=; % cell size in x direction
dy_a=; % cell size in y direction
dz_a=; % cell size in z direction

size_factor=; %expansion ratio of grid

FMAP_y=; %fine_mesh_around_plane y direction
FMAP_z=; %fine_mesh_around_plane z direction



%%%%%%%%%%%%%%%%%%%%%%%%%%%%%%%%%%%%%%%%%%% Flight SETTING

f=; %frequency
m=; % dipole moment
r=; %Spacing between receiver and transmitter
start=; %start point of survey
stop=; %end point of survey
s=; %sample point spacing
```

```
Flight_Altitude=; % Flight Altitude

%%%%%%%%%%%%%%%%%%%%%%%%%%%%%%%%%%%%%%%%%% Physics of the World

anomaly_dimensions= [x y z top]; %% [x y z top depth]
conductivity of the anomaly, air, left and right of the fault in different
directions and etc...
```

Inputs go to different functions such as:

LHS function that creates the derivatives matrices
```
%%%%%%%%%%%%%%%% DEX

center = ones(TN,1); %  0 diagnal (center diagnal)
pos = ones(length(xs),length(ys),length(zs)); % negative diagnal
pos(end,:,:)=zeros(1,length(ys),length(zs));
pos = pos(:);
pos = [0;pos(1:end-1)];
DEX = spdiags([center,pos],[1,1],TN,TN);
```

Curl function that creates Curl operator

```
%%%%%%%%%%%%%%%% Curl

CRL=[sparse(TN,TN)  -DEZ  DEY  ;  DEZ  sparse(TN,TN)  -DEX  ;  -DEY  DEX
sparse(TN,TN)];
```

RHS function that creates primary Fields

```
%%%%%%%%%%%%%%%%% P

for ii=1:length(xs)

    for jj=1:length(ys)

        for kk=1:length(zs)

        r(ii,jj,kk)=((xs(ii)-plane_coordinate(1))^2+(zs(kk)-
z_flight).^2+(ys(jj))^2)^0.5;


Ex_p(ii,jj,kk)=(1i*w*mu*m./(4*pi*(r(ii,jj,kk)).^2)).*(1i.*k.*r(ii,jj,kk)+1).
*(exp(-1i.*k.*r(ii,jj,kk))).*(((ys(jj))./r(ii,jj,kk)));
        Ey_p(ii,jj,kk)=(-
(1i*w*mu*m./(4*pi*(r(ii,jj,kk)).^2)).*(1i.*k.*r(ii,jj,kk)+1).*(exp(-
1i.*k.*r(ii,jj,kk))).*(((xs(ii)-plane_coordinate(1))./r(ii,jj,kk))));

        end
    end
end
```

Create world that creates the world and calculates volume averages based on the cell sizes

```
%%%%%%%% for domain
parfor i=1:length(xs)

    T_si_x=zeros(length(xs),length(ys),length(zs));
```

```
    T_si_y=zeros(length(xs),length(ys),length(zs));
    T_si_z=zeros(length(xs),length(ys),length(zs));


    for j=1:length(ys)
        for k=1:length(zs)


            if i~=1 && i~=length(xs) && j~=1 && j~=length(ys) && k~=1 &&
k~=length(zs)


                T_si_x(i,j,k)=...
                (abs(ys(j)-ys(j-1))/(abs(ys(j)-ys(j+1))+abs(ys(j)-ys(j-1))))*...
                    (abs(zs(k)-zs(k-1))/(abs(zs(k)-zs(k+1))+abs(zs(k)-zs(k-1))))*
elements_x(((k-2)*(length(xs)-1)*(length(ys)-1)+(j-2)*(length(xs)-1)+i),25)+...
                (abs(ys(j)-ys(j+1))/(abs(ys(j)-ys(j+1))+abs(ys(j)-ys(j-1))))*...
                    (abs(zs(k)-zs(k-1))/(abs(zs(k)-zs(k+1))+abs(zs(k)-zs(k-1))))*
elements_x(((k-2)*(length(xs)-1)*(length(ys)-1)+(j-1)*(length(xs)-1)+i),25)+...
                (abs(ys(j)-ys(j-1))/(abs(ys(j)-ys(j+1))+abs(ys(j)-ys(j-1))))*...
                    (abs(zs(k)-zs(k+1))/(abs(zs(k)-zs(k+1))+abs(zs(k)-zs(k-1))))*
elements_x(((k-1)*(length(xs)-1)*(length(ys)-1)+(j-2)*(length(xs)-1)+i),25)+...
                (abs(ys(j)-ys(j+1))/(abs(ys(j)-ys(j+1))+abs(ys(j)-ys(j-1))))*...
                    (abs(zs(k)-zs(k+1))/(abs(zs(k)-zs(k+1))+abs(zs(k)-zs(k-1))))*
elements_x(((k-1)*(length(xs)-1)*(length(ys)-1)+(j-1)*(length(xs)-1)+i),25);
                %%%%%%%%%%%%%%%%%%%%%%%%%%%%%%%%%%%%%
```

4. Validation of Solution

To verify the accuracy of our code for HEM simulations, we compared our results with the finite difference solution of Newman and Alumbaugh, 1995, and integral equation solution of Avdeev *et al*. 1998 for different models.

4.1. 3D target in a half-space

The first model shown in Figure 6 consists of 700by500by500 m including $1\,\Omega m$ body of dimensions 20by200by75 m at depth of 50 m centered at 350 m in a 100 Ωm half-space. HEM configuration: using a vertical magnetic dipole

(VMD) and a horizontal magnetic dipole (HMD) at 900 Hz, flight level is 20 m above the earth's surface. The transmitter and receiver separations are 10 m and the receiver leading the transmitter to the right. In all the examples, the calculation was performed for 29 source positions, and Figure 5 shows the results of the forward midway between transmitter and receiver along the flight line (the line that bisects the body). Figure 5 illustrates the number of equations required to reduce the squared error level to 10^{-8}. As seen in Figure 6, our total field responses are matched well with the Newman curves. Figure 7 shows the secondary magnetic field for a VMD and an HMD position, where the source is located at the top of the conductive body.
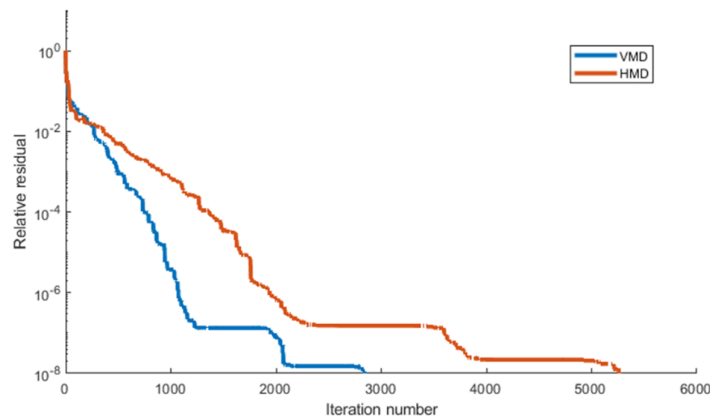

Figure 5. Plot of the relative residual against iteration number for solution of fields based on QMR method.
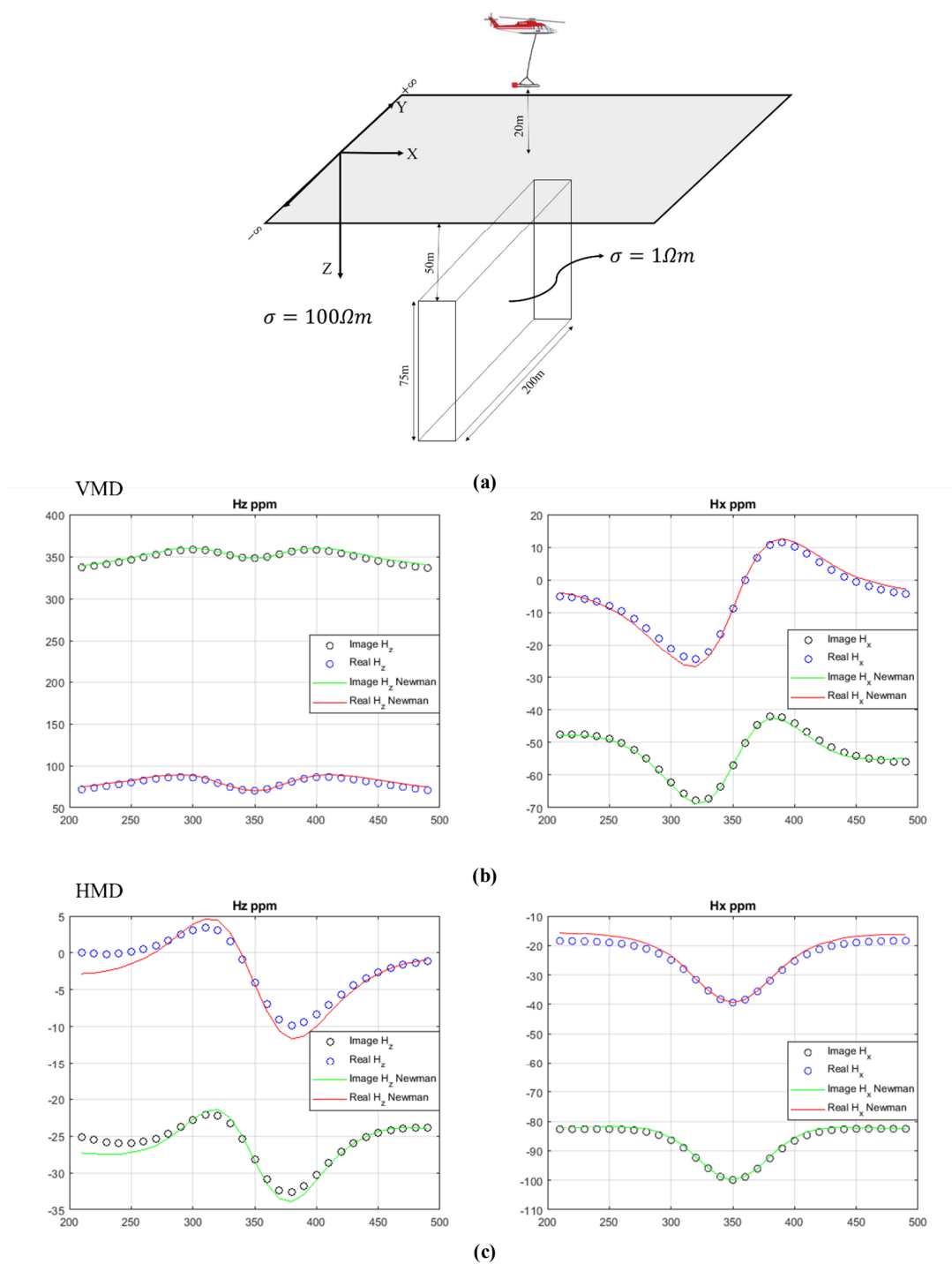
Figure 6. A- 3D body located in 100 Ωm half space B- Comparison of Hx and Hz responses in presence of VMD source calculated with the improved finite difference with Newman results C- Comparison of Hx and Hz responses in presence of HMD source. The fact that larger departures are observed in the real part rather than the imaginary part of the fields indicates that the anomalous body is a good conductor.
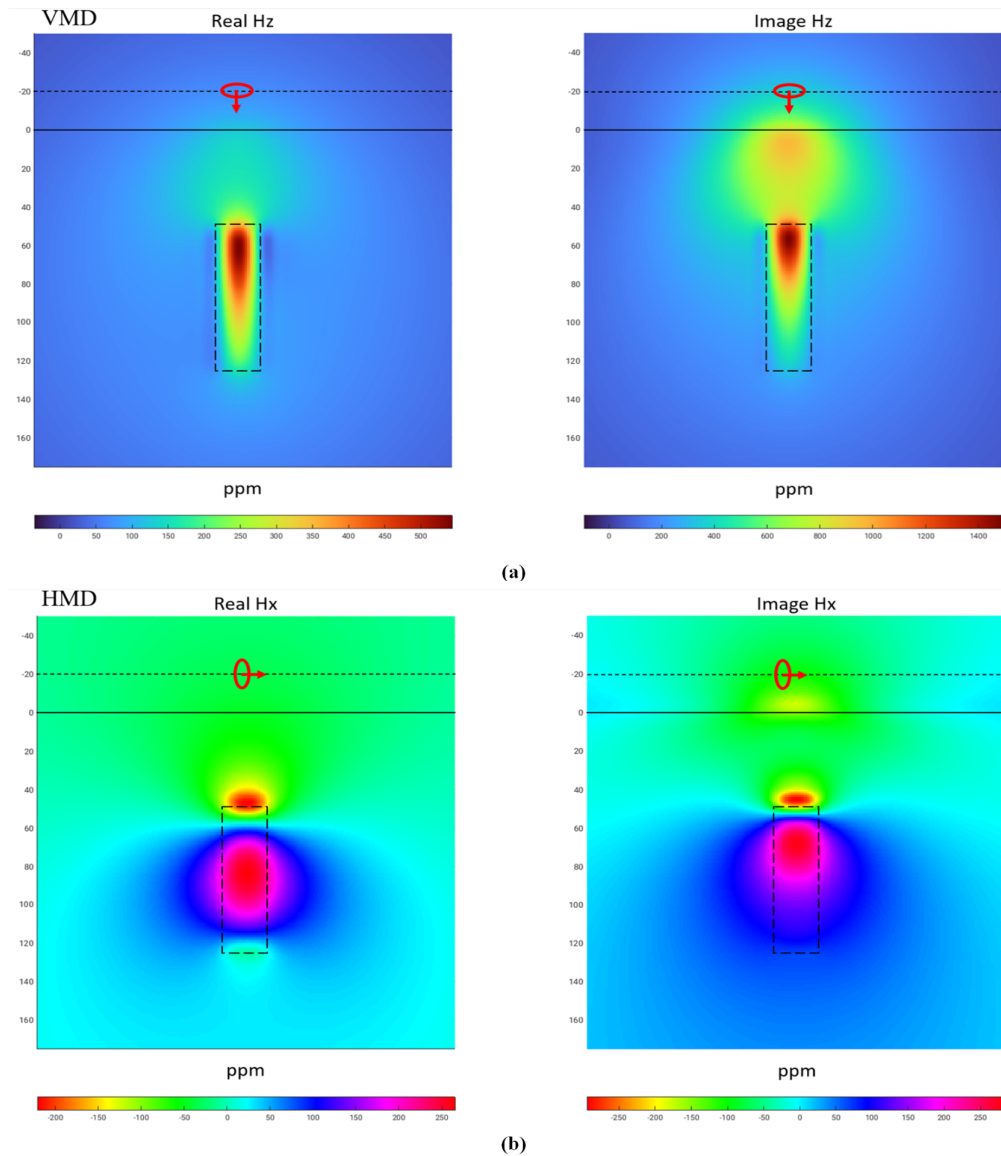
Figure 7. HEM simulation for a 3D body located in 100 Ωm half space. Solid line is Earth-Air border, dashed line is flight path. A. Vertical magnetic-field responses for a VMD source. B. Horizontal magnetic-field responses for an HMD source. As it can be seen, electromagnetic methods are more sensitive to top of the anomalies.

4.2. Vertical fault, anomaly along a vertical fault, and topography

For the next model, we consider faulted half-space consisting of vertical fault at x = 340 m. Resistivity of left side of the fault is $100\,\Omega m$ and right side is $300\,\Omega m$ as shown in Figure 8. In the next step, we add a conductive body with resistivity $1\,\Omega m$ along the vertical fault at depth of 50 m as shown in Figure 9. Model consists of a vertical fault including surface topography as shown in Figure 10. At right of the fault, earth has been thrust 10 m upwards relative to the left side of the fault. The height of the flight has been adjusted so

helicopter keeps the vertical distance to the earth fixed at 20 m.

These figures illustrate how the HEM response of the fault can mask the response of the conductive body. This particularly can be seen in the image component of the fields. To determine if the body is detectable in the presence of the fault, it is necessary to compare responses of the contact with and without the body. This is shown in Figures 8 and 9. Notice that the body produces a detectable anomaly in the real components. Real component is sensitive primarily to conductive body, and because the contact is resistive relative to the body, the fault produces very little real component

response. Thus the real responses of the body in the faulted background are similar to those for a conductor in a resistive half-space. However, notice that the presence of the contact does result in a modest tilt in the profiles of this component. This could possibly be mistaken as an effect of a dipping conductor without any other information being incorporated.

One possible aid to the interpretation is the image part. Although the signature of the body is difficult to detect, particularly in the vertical field inspection of the image response, indicates a rapid change in the host-rock conductivity. This, together with the real response of the conductor, indicates that the conductor sits at or near the fault contact. However, the attitude of the body would be very difficult to conclude without numerical modelling.
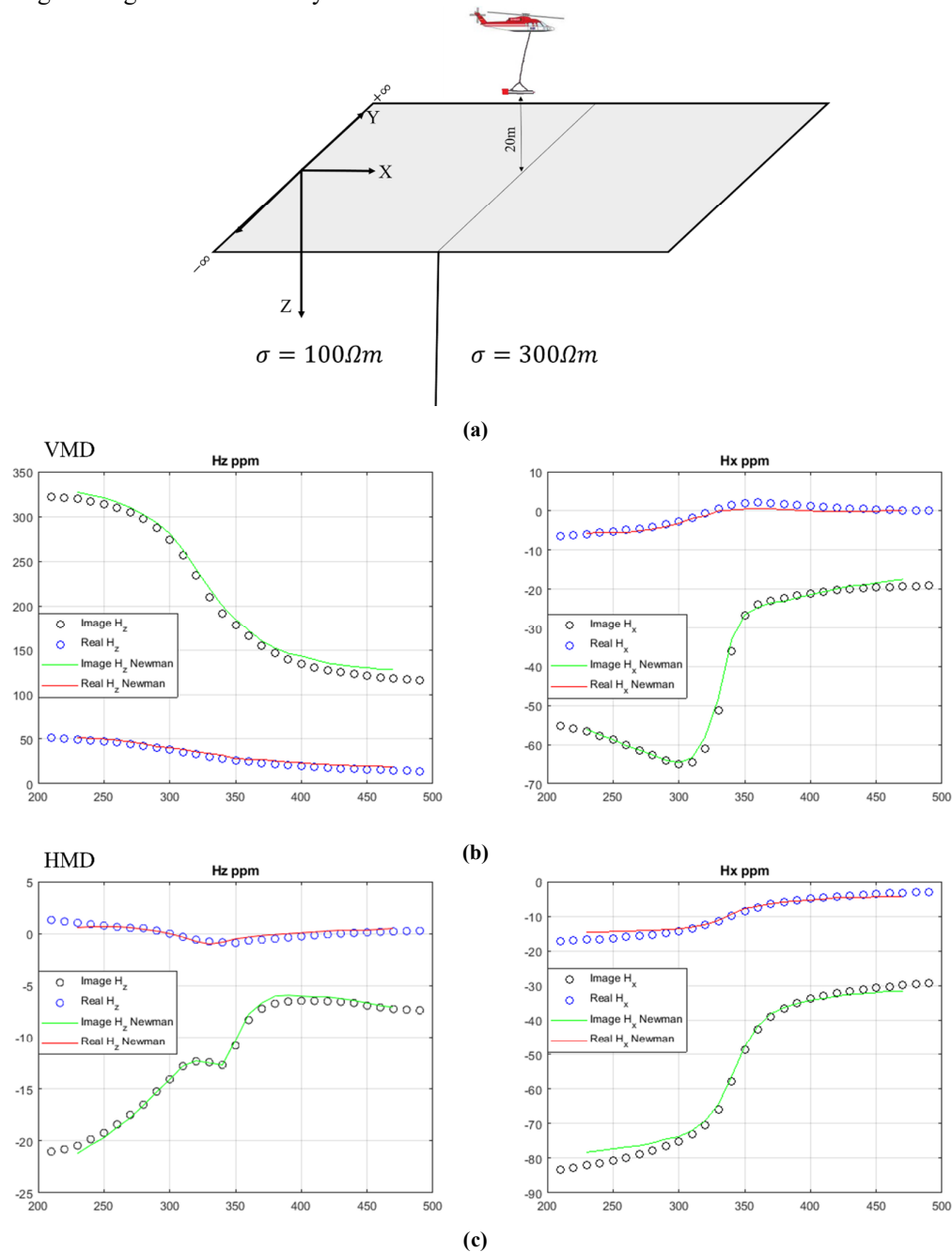

Figure 8. A- Faulted half-space B- Comparison of Hx and Hz responses in presence of VMD source C-Comparison of Hx and Hz responses in presence of HMD source.
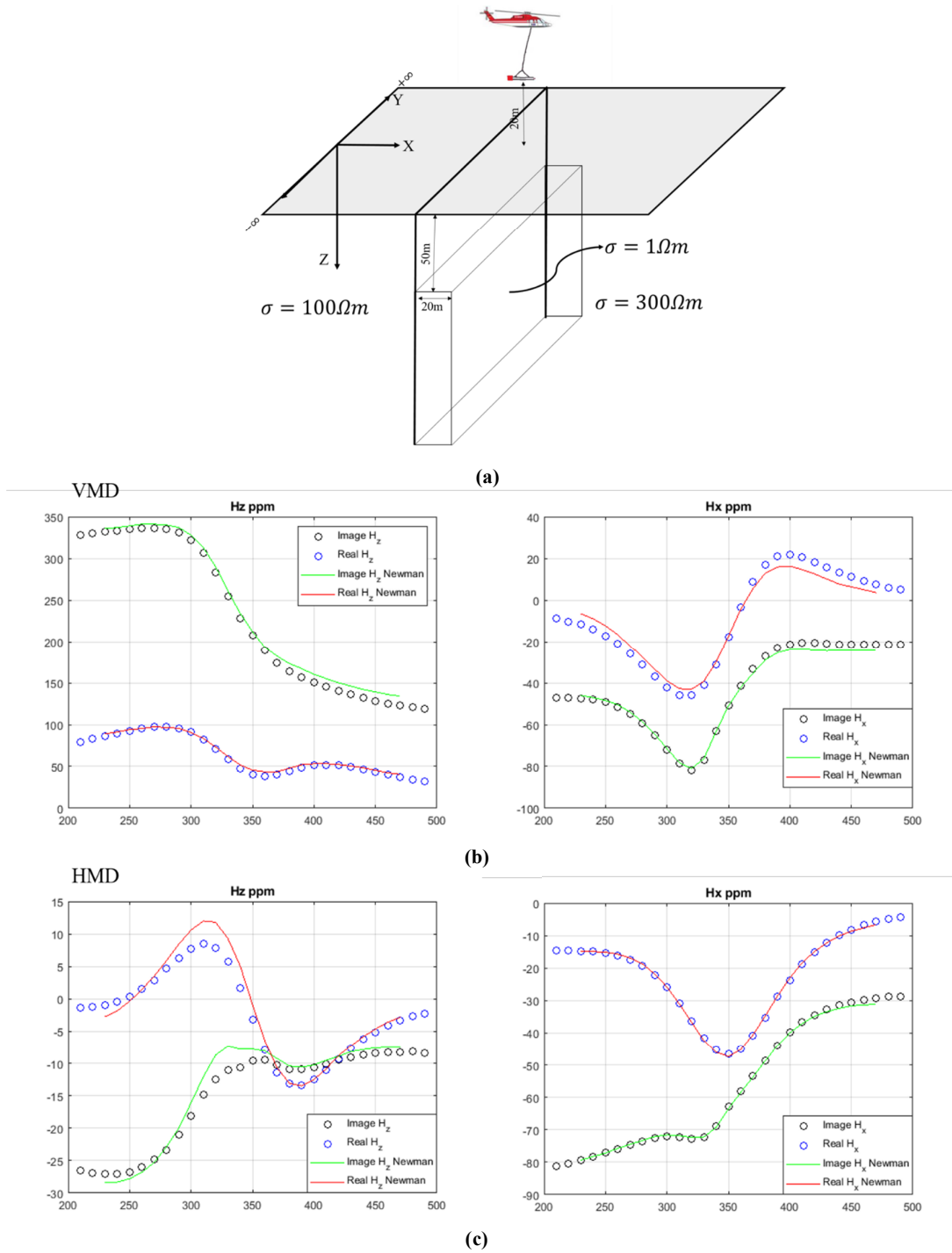
Figure 9. A- 3D body located in faulted half-space B- Comparison of Hx and Hz responses in presence of VMD source calculated with the improved finite difference with Newman results C- Comparison of Hx and Hz responses in presence of HMD source.
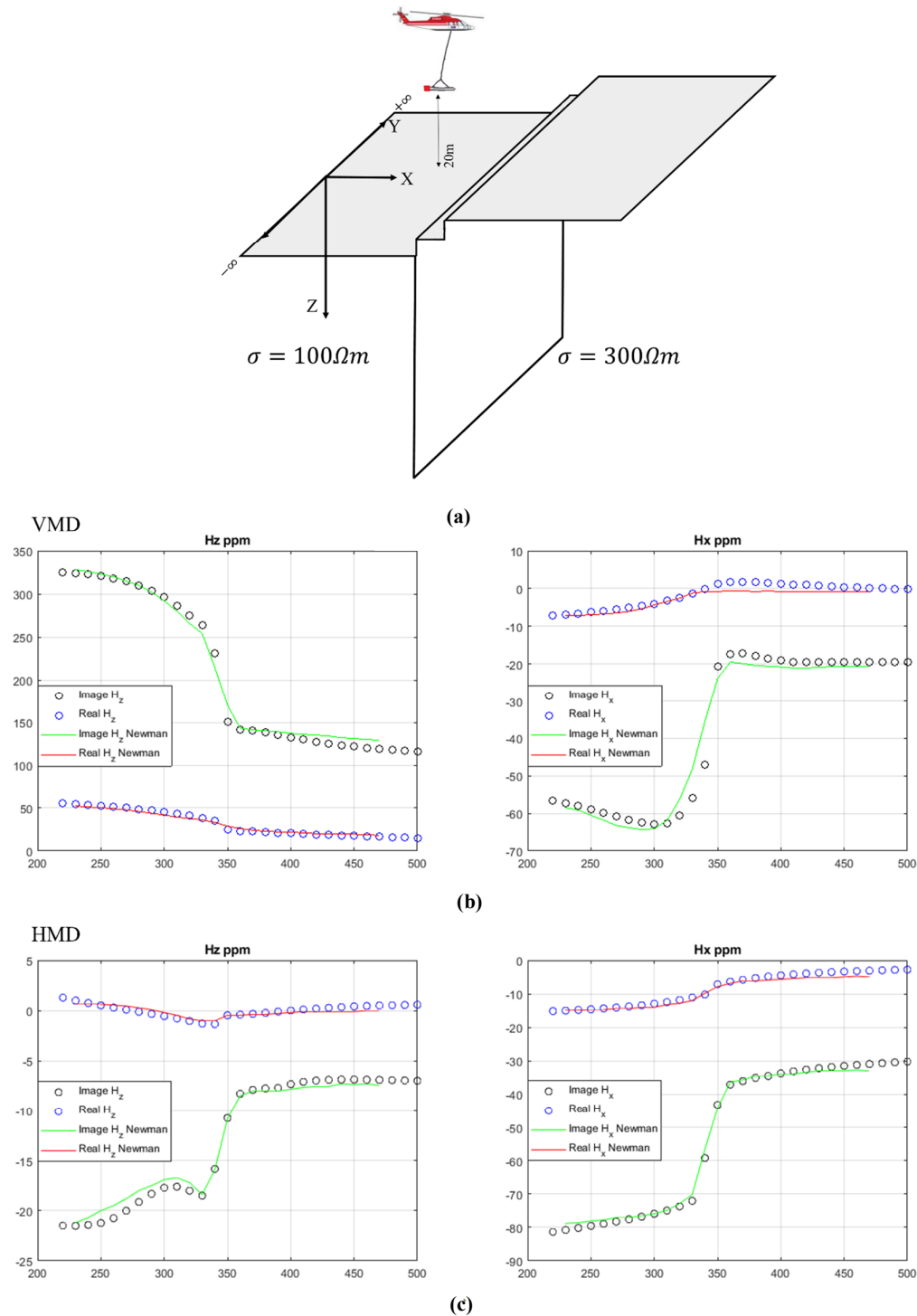
(a)

(b)

(c)

Figure 10. A- Faulted half-space with topography B- Comparison of Hx and Hz responses in presence of VMD source calculated with improved finite difference with Newman results C- Comparison of Hx and Hz responses in presence of HMD source. Effect of the fault and topography is clearly observed in the image responses.

4.3. Anisotropic 3D target in a half-space

At the end, we assume the 3D conductive body is shown in Figure 11. The structure is the same as in Figure 6 but the resistivity of the body is anisotropic, meaning resistivity is different in different directions and represented by a diagonal matrix 26. Anisotropic body is placed in an isotropic $100\,\Omega m$ half-space, and there are three different types of conductive body models to

simulate. Secondary field responses are defined as the difference in the responses of the model with and without the conductive body. We can see some differences between our curves and Avdeev's, and that is because of the different methods we used; Avdeev used the IE solution. Since the body is strike is in the y-direction, the overall induction pattern is naturally governed by the electric

currents flowing along this direction [36], and, consequently, it is controlled by resistivity in the y direction. It is clearly seen from the figures that the amplitudes of the responses damp down significantly when resistivity in y direction increases. The results also show that resistivity in x direction does not affect the responses.
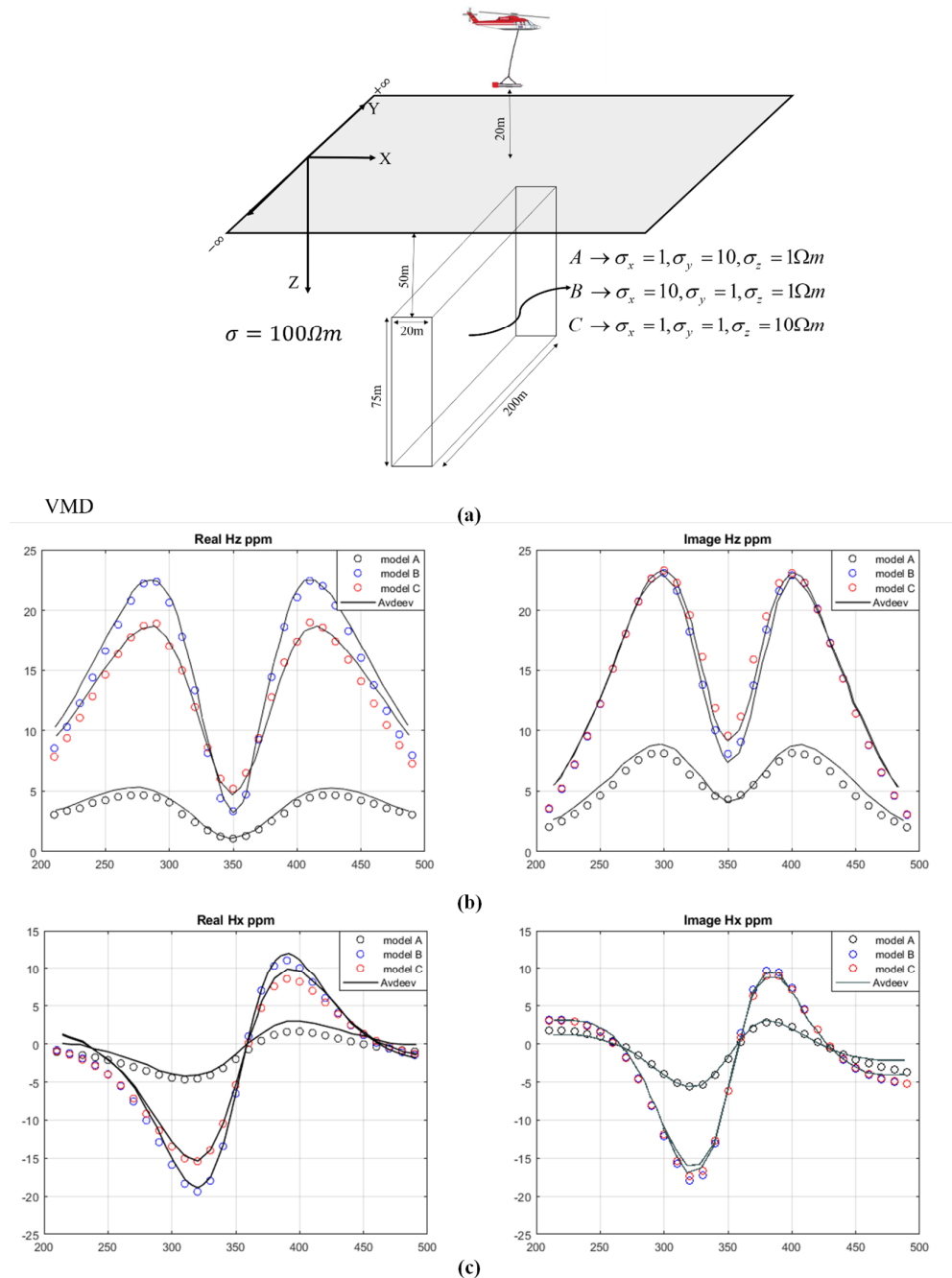

Figure 11. A- 3D body with a different type of resistivity or anisotropy B- Comparison of Hz scattered responses in presence of VMD source calculated with the improved finite difference with Avdeev IE results C- Comparison of Hx scattered responses in presence of VMD source.

5. Conclusions

We implemented two types of MATLAB code based on conventional finite-difference and improved finite-difference to simulate the response of synthetic models in different 2D and 3D models in HEM forward modeling. Both codes give the same answer but the main difference is in the execution time of the code and programming simplicity in the improved finite difference method, so that when air and earth are divided into about 1400000 cells using a grid with dimensions of 700 by 500 by 500 meters, the time required to form a stiffness matrix in the conventional method is about 25000 seconds but in the improved method this time is less than 30 seconds is a big difference. In terms of Ram usage, improved method used 48 GB of Ram for 14 and 3 seconds but the conventional method used 48 GB of Ram for almost 7 hours; on the other hand, because we use sparse matrices throughout the code, it only requires less than 100 MB of memory space, compared to conventional matrices that require more than 15 GB. Comparison of the results of this study with previous articles shows a very good match of the results.

References

[1]. Peltoniemi, M. (1998). Depth of penetration of frequency-domain airborne electromagnetics in resistive terrains. Exploration Geophysics. 29 (2): 12-15.

[2]. Tan, K., Munday, T., Halas, L., and Cahill, K. (2009). Utilizing airborne electromagnetic data to map groundwater salinity and salt store at Chowilla, SA. ASEG Extended Abstracts. 2009 (1): 1-6.

[3]. Siemon, B., Steuer, A., Ullmann, A., Vasterling, M., and Voß, W. (2011). Application of frequency-domain helicopter-borne electromagnetics for groundwater exploration in urban areas. Physics and Chemistry of the Earth, Parts A/B/C. 36 (16): 1373-1385.

[4]. Baranwal, V. C., Brönner, M., Rønning, J. S., Elvebakk, H., and Dalsegg, E. (2020). 3D interpretation of helicopter-borne frequency-domain electromagnetic (HEM) data from Ramså Basin and adjacent areas at Andøya, Norway. Earth, Planets and Space. 72 (1): 1-14.

[5]. Huang, H. and Fraser, D.C. (1996). The differential parameter method for multi-frequency airborne resistivity mapping. Geophysics 61 (1): 100–109.

[6]. Farquharson, C.G., Oldenburg, D.W., and Routh, P.S. (2003). Simultaneous 1D inversion of loop–loop electromagnetic data for magnetic susceptibility and electrical conductivity. Geophysics. 68 (6): 1857-1869.

[7]. Yin, C. and Hodges, G. (2007). Simulated annealing for airborne EM inversion. Geophysics 72 (4): F189–F195.

[8]. Arab-Amiri, A.R., Moradzadeh, A., Fathianpour, N., and Siemon, B. (2011). Inverse modeling of HEM data using a new inversion algorithm. JME. 1 (2): 9–20.

[9]. Siemon, B. (2012). Accurate 1D forward and inverse modeling of high-frequency helicopter-borne electromagnetic data. Geophysics .77 (4): WB71–WB87.

[10]. Lin, C., Fiandaca, G., Auken, E., Couto, M. A., and Christiansen, A.V. (2019). A discussion of 2D induced polarization effects in airborne electromagnetic and inversion with a robust 1D laterally constrained inversion scheme. Geophysics. 84 (2): E75-E88.

[11]. Sharifi, F., Arab-Amiri, A.R., Kamkar-Rouhani, A., and Börner, R.U. (2019). One-Dimensional Modeling of Helicopter-Borne Electromagnetic Data Using Marquardt-Levenberg Including Backtracking-Armijo Line Search Strategy. International Journal of Mining and Geo-Engineering. 53 (2): 143-150.

[12]. Sharifi, F., Arab-Amiri, A.R., Kamkar-Rouhani, A., and Börner, R.U. (2020). Development of a novel approach for recovering SIP effects from 1-D inversion of HEM data: Case study from the Alut area, northwest of Iran. Journal of Applied Geophysics, 174, 103962.

[13]. Mitsuhata, Y. (2000). 2-D electromagnetic modeling by finite-element method with a dipole source and topography. Geophysics. 65 (2): 465-475.

[14]. Mitsuhata, Y., Uchida, T., and Amano, H. (2002). 2.5-D inversion of frequency-domain electromagnetic data generated by a grounded-wire source. Geophysics. 67 (6): 1753-1768.

[15]. Abubakar, A., Habashy, T.M., Druskin, V.L., Knizhnerman, L., and Alumbaugh, D. (2008). 2.5 D forward and inverse modeling for interpreting low-frequency electromagnetic measurements. Geophysics. 73 (4): F165-F177.

[16]. Ramananjaona, C. and MacGregor, L. (2010, November). 2.5 D inversion of CSEM data in a vertically anisotropic earth. In Journal of Physics: Conference Series (Vol. 255, No. 1, p. 012004). IOP Publishing.

[17]. Key, K. and Ovall, J. (2011). A parallel goal-oriented adaptive finite element method for 2.5-D electromagnetic modelling. Geophysical Journal International. 186 (1): 137-154.

[18]. Streich, R., Becken, M., and Ritter, O. (2011). 2.5 D controlled-source EM modeling with general 3D source geometries. Geophysics. 76 (6): F387-F393.

[19]. Li, W.B., Zeng, Z.F., Li, J., Chen, X., Wang, K., and Xia, Z. (2016). 2.5 D forward modeling and

inversion of frequency-domain airborne electromagnetic data. Applied Geophysics. 13 (1): 37-47.

[20]. Boesen, T., Auken, E., Christiansen, A. V., Fiandaca, G., Kirkegaard, C., Aspmo Pfaffhuber, A., and Vöge, M. (2018). An efficient 2D inversion scheme for airborne frequency-domain data. Geophysics, 83(4): E189-E201.

[21]. Cheng, J., Xue, J., Zhou, J., Dong, Y., and Wen, L. (2019). 2.5-D inversion of advanced detection transient electromagnetic method in full space. IEEE Access, 8, 4972-4979.

[22]. Ghari, H.A., Voge, M., Bastani, M., Pfaffhuber, A.A., and Oskooi, B. (2020). Comparing resistivity models from 2D and 1D inversion of frequency domain HEM data over rough terrains: cases study from Iran and Norway. Exploration Geophysics. 51 (1): 45-65.

[23]. Idesman, A. and Dey, B. (2020). A new numerical approach to the solution of the 2-D Helmholtz equation with optimal accuracy on irregular domains and Cartesian meshes. Computational Mechanics. 65 (4): 1189-1204.

[24]. Li, G., Duan, S., Cai, H., Han, B., and Ye, Y. (2020). Improved interpolation scheme at receiver positions for 2.5 D frequency-domain marine CSEM forward modelling. In EGU General Assembly Conference Abstracts (p. 20994).

[25]. Avdeev, D.B. (2005). Three-dimensional electromagnetic modelling and inversion from theory to application: Surveys in Geophysics, 26, 767–799, doi: 10.1007/s10712-005-1836-x.

[26]. Zhdanov, M.S. (2009). Geophysical electromagnetic theory and methods: Elsevier.

[27]. Börner, R.U. (2010). Numerical modeling in geo-electromagnetics: Advances and challenges: Surveys in Geophysics, 31, 225–245, doi: 10.1007/s10712-009-9087-x.

[28]. Koldan, J. (2013). Numerical solution of 3-D electromagnetic problems in exploration geophysics and its implementation on massively parallel computers.

[29]. Scheunert, M. (2015). 3-D inversion of helicopter-borne electromagnetic data. PhD dissertation, TU Bergakademie Freiberg.

[30]. Dunham, M.W., Ansari, S., and Farquharson, C.G. (2018). Application of 3D marine controlled-source electromagnetic finite-element forward modeling to hydrocarbon exploration in the Flemish Pass Basin offshore Newfoundland, Canada. Geophysics. 83 (2): WB33-WB49.

[31]. Coggon, J.H. (1971). Electromagnetic and electrical modeling by the finite element method. Geophysics, 36(1): 132-155.

[32]. Xiong, Z. (1992). Electromagnetic modeling of 3-D structures by the method of system iteration using integral equations. Geophysics. 57 (12): 1556-1561.

[33]. Newman, Gregory A., and David L. Alumbaugh (1995). "Frequency-domain Modelling of Airborne Electromagnetic Responses using Staggered Finite Differences". In: Geophysical Prospecting 43, lO21–1O42.

[34]. Habashy, T.M., Groom, R.W., and Spies, B.R. (1993). Beyond the Born and Rytov approximations: A non-linear approach to electromagnetic scattering. Journal of Geophysical Research: Solid Earth. 98 (B2): 1759-1775.

[35]. Traynin, P., Zhdanov, M.S., Nyquist, J., Beard, L., and Doll, W. (1996). A new approach to interpretation of airborne magnetic and electromagnetic data: Proceedings of SAGEEP 96, Environmental and Engineering Geophysical Society.

[36]. Avdeev, D.B., Kuvshinov, A.V., Pankratov, O.V., and Newman, G.A. (1998). Three-dimensional frequency-domain modeling of airborne electromagnetic responses. Exploration Geophysics. 29 (1-2): 111-119.

[37]. Zhdanov, M. and Hursan, G. (2000). 3D electromagnetic inversion based on quasi-analytical approximation. Inverse Problems. 16 (5): 1297.

[38]. Pfaffhuber, A.A., Hendricks, S., and Kvistedal, Y.A. (2012). Progressing from 1D to 2D and 3D near-surface airborne electromagnetic mapping with a multisensor, airborne sea-ice explorer. Geophysics. 77 (4): WB109-WB117.

[39]. Cox, L.H., Wilson, G.A., and M.S. Zhdanov (2010): 3D inversion of airborne electromagnetic data using a moving footprint: Exploration Geophysics, 41, 250-259.

[40]. Scheunert, M., Ullmann, A., Afanasjew, M., Börner, R.U., Siemon, B., and Spitzer, K. (2016). 3D Inversion of Helicopter-borne Electromagnetic Data-A Cut-&-Paste Strategy. In 78th EAGE Conference and Exhibition 2016 (Vol. 2016, No. 1, pp. 1-5). European Association of Geoscientists & Engineers.

[41]. Jang, H., Cho, S.O., Kim, B., Kim, H. J., and Nam, M.J. (2021). Three-dimensional finite-difference modeling of time-domain electromagnetic responses for a large-loop source. Geosciences Journal. 25 (5): 675-684.

[42]. Yin, C., Zhang, B., Liu, Y., and Cai, J. (2016). A goal-oriented adaptive finite-element method for 3D scattered airborne electromagnetic method modeling. Geophysics. 81 (5): E337-E346.

[43]. Li, J., Farquharson, C. G., and Hu, X. (2017). 3D vector finite-element electromagnetic forward modeling for large loop sources using a total-field algorithm and unstructured tetrahedral grids. Geophysics. 82 (1): E1-E16.

[44]. Castillo Reyes, O. (2017). Edge-elements formulation of 3D CSEM in geophysics: a parallel approach.

[45]. Huo, Z., Zeng, Z., Li, J., Li, W., Zhang, L., and Wang, K. (2019). 3D non-linear conjugate gradient inversion for frequency-domain airborne EM based on vector finite element method. In SEG Technical Program Expanded Abstracts 2019 (pp. 2928-2932). Society of Exploration Geophysicists.

[46]. Haber, E. (2014). Computational methods in geophysical electromagnetics. Society for Industrial and Applied Mathematics.

[47]. Jahandari, H. and Farquharson, C.G. (2015). Finite-volume modelling of geophysical electromagnetic data on unstructured grids using potentials. Geophysical Journal International. 202 (3): 1859-1876.

[48]. Jahandari, H., Ansari, S., and Farquharson, C.G. (2017). Comparison between staggered grid finite–volume and edge–based finite–element modelling of geophysical electromagnetic data on unstructured grids. Journal of Applied Geophysics, 138, 185-197.

[49]. Lu, X. and Farquharson, C.G. (2020). 3D finite-volume time-domain modeling of geophysical electromagnetic data on unstructured grids using potentials. Geophysics. 85 (6): E221-E240.

[50]. Jahandari, H. and Bihlo, A. (2021). Forward modelling of geophysical electromagnetic data on unstructured grids using an adaptive mimetic finite-difference method. Computational Geosciences. 25 (3): 1083-1104.

[51]. Farquharson, C.G. and Oldenburg, D. (2002). Chapter 1 An integral equation solution to the geophysical electromagnetic forward-modelling problem. Methods in geochemistry and geophysics, 35, 3-19.

[52]. Zhdanov M. S., F.A. Alfouzan, L. Cox, A. Alotaibi,, M. Alyousif, D. Sunwall, and M. Endo (2018): Large-scale 3D Modeling and Inversion of Multiphysics Airborne Geophysical Data: A Case Study from the Arabian Shield, Saudi Arabia: Minerals, 8, 271; doi:10.3390/min8070271.

[53]. Yoon, D., Zhdanov, M.S., Mattsson, J., Cai, H., and Gribenko, A. (2016). A hybrid finite-difference and integral-equation method for modeling and inversion of marine controlled-source electromagnetic data. Geophysics. 81 (5): E323-E336.

[54]. Sarakorn, W., and Vachiratienchai, C. (2018). Hybrid finite difference–finite element method to incorporate topography and bathymetry for two-dimensional magnetotelluric modeling. Earth, Planets and Space. 70 (1): 103.

[55]. Varilsuha, D. and Candansayar, M.E. (2018). 3D magnetotelluric modeling by using finite-difference method: Comparison study of different forward modeling approaches. Geophysics. 83 (2): WB51-WB60.

[56]. van't Hof, B. and Vuik, M.J. (2019). Symmetry-preserving finite-difference discretizations of arbitrary order on structured curvilinear staggered grids. Journal of Computational Science, 36, 101008.

[57]. Yee, K. (1966). Numerical solution of initial boundary value problems involving Maxwell's equations in isotropic media. IEEE Transactions on antennas and propagation. 14 (3): 302-307.

[58]. Gilles, L., Hagness, S.C., and Vázquez, L. (2000). Comparison between staggered and unstaggered finite-difference time-domain grids for few-cycle temporal optical soliton propagation. Journal of Computational Physics. 161 (2): 379-400.

[59]. Rumpf, R.C. (2012). Simple implementation of arbitrarily shaped total-field/scattered-field regions in finite-difference frequency-domain. Progress in Electromagnetics Research, 36, 221-248.

[60]. Rumpf, R. C., Garcia, C. R., Berry, E. A., and Barton, J. H. (2014). Finite-difference frequency-domain algorithm for modeling electromagnetic scattering from general anisotropic objects. Progress in Electromagnetics Research B, 61, 55-67.

[61]. Ward, Stanley H. and Gerald W. Hohmann (1988). "Electromagnetic Theory for Geophysical Applications". In: Electromagnetic Methods in Applied Geophysics. Ed. by M. N. Nabighian. Vol. 1, Theory. Investigations in Geophysics 3. Society of Exploration Geophysicists, pp. 130–311.

[62]. Lowry, T., M. B. Allen, and P. N. Shive (1989). "Singularity Removal: A Refinement of Resistivity Modeling Techniques". In: Geophysics 54, pp. 766–774.

[63] Sarkar TK. (1987) On the application of the generalized biconjugate gradient method, Journal of Electromagnetic Waves and Applications, 1, 223-242.

[64]. Smith CF, Peterson AF, and Mittra R, (1990): The biconjugate gradient method for electromagnetic scattering, IEEE Trans. Antennas Propagat., Vol. 38, pp. 938–940.

[65]. Wang, C.F. and Jin, J.M. (1998): Simple and efficient computation of electromagnetic fields in arbitrarily shaped inhomogeneous dielectric bodies using transpose-free QMR and FFT, IEEE Transactions on Microwave Theory and Techniques, vol.46, no.5, pp.553-558.

[66]. De Gersem H., Lahaye D, Vandewalle S, and Hameyer K (1999). Comparison of quasi minimal residual and bi-conjugate gradient iterative methods to solve complex symmetric systems arising from time-harmonic simulations, COMPEL, 18, 3, 298-310.

[67]. Alumbaugh, D. L., G.A. Newman, L. Prevost, and J.N. Shadid (1996). Three-dimensional wideband

electromagnetic modeling on massively parallel computers, Radio Science, 31, 1-23.

[68]. Siemon, Bernhard, Anders Vest Christiansen, and Esben Auken (2009). "A Review of Helicopter-borne Electromagnetic Methods for Groundwater Exploration". In: Near Surface Geophysics 7, pp. 629–646.

مدل‌سازی مستقیم داده‌های الکترومغناطیس هلیکوپتری حوزه فرکانس با استفاده از روش تفاضلات محدود بهبود یافته

سعید نظری، علیرضا عرب‌امیری*، ابوالقاسم کامکار روحانی و فریدون شریفی

دانشکده مهندسی معدن، نفت و ژئوفیزیک، دانشگاه صنعتی شاهرود، سمنان، ایران

* نویسنده مسئول مکاتبات:alirezaarabamiri@yahoo.com

چکیده:

در این مطالعه، ما داده‌های الکترومغناطیسی هوابرد هلیکوپتری (HEM) حوزه فرکانس را بر روی مدل‌های زمین دو بعدی (2D) و سه بعدی (3D) حاوی یک ناهنجاری در حضور منبع دوقطبی مغناطیسی شبیه‌سازی می‌کنیم. برای دستیابی به این امر، از معادله بردار هلمهولتز برای جلوگیری از مشکلات همگرایی در معادلات ماکسول استفاده می‌شود و میدان‌ها به اولیه و ثانویه تقسیم می‌شوند. ما از روش تفاضل محدود به صورت ناهم مبدا برای گسسته کردن معادلات استفاده می‌کنیم که می‌تواند به دو صورت انجام شود، از جمله روش‌های تفاضل محدود معمولی (مرسوم) و بهبود یافته. روش مرسوم از نظر برنامه نویسی بسیار پیچیده است که باعث ایجاد خطا در برنامه نویسی می‌شود. علاوه بر این، به حلقه‌های برنامه نویسی (for loops) متفاوتی نیاز دارد که این حلقه‌ها باید برای هر نقطه از شبکه تکرار شوند که باعث افزایش زمان اجرای برنامه می‌شود. روش دوم تفاضل محدود بهبود یافته (IFDM) است که در آن از ماتریس‌های مشتق از پیش ساخته شده استفاده می‌کنیم. می‌توانیم این ماتریس‌های مشتق از پیش ساخته شده را در معادلات مشتق جایگزین کنیم و آن‌ها را مستقیماً از فرم دیفرانسیلی به شکل ماتریسی تبدیل کنیم. این روش باعث می‌شود هر معادله‌ای به صورت دیفرانسیلی با درجات مختلف و پیچیدگی‌های متفاوت باشد را به سادگی به یک فرم ماتریسی تبدیل کنیم. پس از به دست آوردن فرم ماتریسی، سیستم معادلات خطی مانند Ax=b به دست می‌آید که آن را می‌توان با روش‌های تکراری یا مستقیم حل کرد. این روش بسیار ساده است و پیچیدگی‌های روش مرسوم را ندارد و برای تشکیل ماتریس سختی یا ضرایب به زمان اجرای بسیار کمتری نیاز دارد. علاوه بر این، فرآیند برنامه نویسی آن بسیار ساده است. برای حل سیستم معادلات خطی از روش تکراری شبه حداقل باقیمانده (QMR) استفاده شده است. برای اعتبارسنجی روش، نتایج خود را با مدل‌های مختلف مقایسه کردیم، از جمله مدل‌های رسانا سه‌بعدی، مدل‌های دوبعدی مانند مدل گسل‌دار با و بدون جسم رسانا، مدل دوبعدی با توپوگرافی و در نهایت مدل سه‌بعدی حاوی رسانا با رسانایی ناهمسانگرد که در مقایسه با حل FDM نیومن و حل معادلات انتگرال Avdeev برازش خوبی را نشان داد.

کلمات کلیدی: الکترومغناطیس هلیکوپتری، حوزه فرکانس، مدل‌سازی مستقیم، روش تفاضلات محدود.